Molecular Vision 2007; 13:273-86 <http://www.molvis.org/molvis/v13/a31/>
Received 29 November 2005 | Accepted 15 February 2007 | Published 27 February 2007

Defects in retinal pigment epithelium cell proliferation and retinal attachment in mutant mice with *p27^{Kip1}* gene ablation

Dennis M. Defoe,[1] Lorrie B. S. Adams,[1] Jingru Sun,[1,2] Sarah N. Wisecarver,[1] Edward M. Levine[3]

[1]Department of Anatomy and Cell Biology, [2]Graduate Biomedical Research Program, James H. Quillen College of Medicine, East Tennessee State University, Johnson City, TN, [3]Department of Ophthalmology and Visual Sciences, University of Utah School of Medicine, Salt Lake City, UT

Purpose: Little is known about the mechanisms that regulate cell cycle withdrawal of the retinal pigment epithelium (RPE) during development, or about the mechanisms maintaining epithelial cell quiescence in adult retinas. The present study examines the potential role of the negative cell cycle regulator p27^{Kip1} in controlling RPE proliferation, using mice with targeted ablation of the *p27^{Kip1}* gene.

Methods: Ocular tissues were obtained from wild-type and *p27^{Kip1}*-null mice at several postnatal ages. Following aldehyde fixation, eyes were processed intact for JB-4 histology and electron microscopy. Alternatively, tissues were removed by manual or enzymatic dissection in order to obtain flat-mounts of the RPE attached to either the choroid-sclera or neural retina, respectively. Epithelial flat-mounts were either left unlabeled, in which case melanin pigment provided internal contrast, or labeled with Alexa Fluor 488-phalloidin and propidium iodide to visualize cell boundaries and nuclei, respectively.

Results: Morphometric analysis using transverse plastic sections revealed a 96% increase in nuclear density and a 12% increase in thickness (apical to basal) for mutant vs. normal epithelia at postnatal day 35 (P35). These changes were not restricted to central or peripheral regions, and were uncorrelated with focal areas of dysplasia seen in the mutant neural retina. When similar tissues were viewed as flat-mounts, an observed 100% increase in nuclear density was accompanied by only a 46% enhancement in cellular density. This resulted in a larger proportion of multinucleated cells in the nullizygous RPE as compared with the wild-type epithelium (91 versus 47%). Such a pattern was achieved relatively early in development since, at P7 when the increase in RPE nuclear density was essentially complete, cellular density was augmented by only 39%. In addition to these proliferative changes, individual epithelial cells sometimes exhibited structural abnormalities, including an altered cortical actin cytoskeleton and displacement of nuclei from their normal central position. Surprisingly, while the RPE cells of null animals were similar ultrastructurally to those of the wild-type, interdigitation of their microvillous processes with outer segments was incomplete. Quantitative analysis revealed that such areas of detachment characterize, on average, 42% of the nullizygous retina, and that there is little correlation between detachment and neural retina dysplasia from one eye to another. Together with parallel evidence demonstrating a substantial decline in the apparent adhesiveness of mutant retinas relative to the normal tissue, the data is strongly indicative of an altered epithelium-photoreceptor interaction following gene ablation.

Conclusions: The absence of a functional *p27^{Kip1}* gene results in enhanced RPE nuclear division, without a commensurate increase in cell division. Although the mutant epithelium as a whole appears structurally normal, individual cells exhibit cytoskeletal changes and their interaction with the neural retina is compromised.

The retinal pigment epithelium (RPE), a monolayer of cells situated between the vascular choroid and neural retina, provides critical support for photoreceptor cells, the rods and cones. Not only is the epithelium responsible for regulating the extracellular environment of the outer retina, it also helps to maintain photoreceptor function by participating in visual pigment regeneration, disc membrane turnover and the scavenging of free radicals [1,2]. In the mature retina, the level of support afforded by the epithelium depends critically upon the number or density of cells that reside within the monolayer. This is especially evident in diseases characterized by epithelial cell loss, such as macular degeneration and injury-induced atrophy of the RPE, in which there is a gradual decline in many retinal functions [3,4]. Because mature RPE cells are essentially post-mitotic, and a robust stem cell population which could replace damaged cells apparently does not exist, the epithelium is particularly dependent upon mechanisms determining cell number during development. Clearly, those cells generated in the fetus must last a lifetime.

In many vertebrate cell lineages, precursor cells divide a limited number of times before they exit the cell cycle and terminally differentiate. The cell divisions are driven by extracellular signals (mitogens), which alter the expression or

Correspondence to: Dennis M. Defoe, Department of Anatomy and Cell Biology, James H. Quillen College of Medicine, East Tennessee State University, Johnson City, TN 37614-0582; Phone: (423) 439-2010; FAX: (423) 439-2017; email: defoe@etsu.edu

Ms. Wisecarver is now in the Graduate Program, Department of Biochemistry, Cellular and Molecular Biology, University of Tennessee, Knoxville, TN. Ms. Sun is now at the Department of Microbiology and Graduate Biomedical Research Program, James H. Quillen College of Medicine, East Tennessee State University, Johnson City, TN.

activity of regulatory proteins comprising the core cell cycle machinery. These include a set of cyclin-dependent kinases (Cdks), which are cyclically activated to trigger different phases of the cell cycle [5,6], as well as additional proteins that influence Cdk activity in a positive or negative manner [7,8]. Cyclins are stimulatory Cdk-binding co-factors, and D-type cyclins in particular mediate mitogen-dependent progression of cells through a restriction point in the G1 phase of the cycle [6]. An important class of inhibitory cell cycle proteins is the Cdk inhibitors, of which there are two main families, the Ink4 family and Cip/Kip family [9]. Current evidence suggests that Cdk inhibitors might have important roles in regulating the timing of exit from the mitosis prior to cell differentiation [10,11]. The inhibitor $p27^{Kip1}$, in particular, has been proposed to be part of a cell-intrinsic timer that arrests the cell cycle and initiates differentiation in a number of lineages [12,13].

Several groups have reported gigantism and multi-organ hyperplasia in mice with targeted disruption of the *p27Kip1* gene [14-16]. Some of the most dramatic phenotypic changes in these animals are seen in the retina. For example, the neural retina exhibits focal areas of dysplasia, attributed to extended histogenesis of photoreceptors and Müller cells and to the displacement of reactive glia into the layer of photoreceptor outer segments, leading to a disruption in the normal organization of the outer nuclear layer [17,18]. In these same animals, it has been reported that the RPE exhibits an increase in thickness, in its apical to basal dimension, compared to that which is seen in the congenic C57BL/6J strain [16]. We have examined this difference in more detail, in order to assess whether $p27^{Kip1}$ plays a role in determining epithelial cell number. Our results not only indicate that $p27^{Kip1}$ is an important factor regulating RPE proliferation during development, but also that this protein may be a crucial factor involved in generating appropriately polarized epithelial cells and in the construction of the photoreceptor-RPE interface.

METHODS

Mice and genotyping: Hemizygous *p27Kip1* mice (+/-), on a C57BL/6 background [14], were purchased from The Jackson Laboratory (Bar Harbor, ME) and used to set up a breeding colony. Animals were housed in the Animal Care Facilities at ETSU College of Medicine in accordance with Association of Assessment and Accreditation of Laboratory Animal Care (AAALAC) guidelines. Tail snips were taken from all mice on or before 4 weeks of age and genomic DNA extracted and purified using a DNeasy Tissue Kit (Qiagen Inc., Valencia, CA). Genotypes were determined by performing PCR amplification of the wild-type and mutant *p27Kip1* alleles [14]. One common sense primer (5'-TGG AAC CCT GTG CCA TCT CTA T) was used to detect both alleles, while the antisense primers employed were specific for the wild-type allele (5'-GAG CAG ACG CCC AAG AAG C) and the *neo*-disrupted allele (5'-CCT TCT ATG GCC TTC TTG ACG). PCR was performed for 40 cycles with an annealing temperature of 55 °C [19]. Oligonucleotide products were then resolved on a 2% agarose gel and visualized after staining with Sybr Gold (Molecular Probes, Eugene, OR). The wild-type allele resulted in amplification of a 1300-bp product and the null allele a 600-bp product [14]. The results of PCR analysis were independently verified by immunoblotting, using a monoclonal anti-$p27^{Kip1}$ antibody and neural tissues dissected from the brains of neonatal animals, as previously described [20].

Histological analysis and electron microscopy: Mice were euthanized by CO_2 asphyxiation and the enucleated eyes immersion-fixed overnight in 4% glutaraldehyde in 0.1 M phosphate buffer, pH 7.4. The following day, specimens were rinsed several times in buffer in preparation for plastic embedding. Unless otherwise noted, globes were left undissected in order to minimize the possibility of retinal detachment. For routine histology, tissues were dehydrated in graded ethanols prior to infiltration in JB-4 embedding medium (EM Sciences, Hatfield, PA). Polymerization was carried out according to the manufacturer's instructions and tissue blocks stored under dessicant until used. Relatively thick (3 μm) sections were obtained in a vertical plane through the middle of the eye and stained with Azure II-methylene blue. For documentation, digital images of the stained sections were taken using an Olympus BX41 microscope equipped with a 40X objective and an Optronics MagnaFire SP CCD camera, and processed using Photoshop CS2 (Adobe Systems, San Jose, CA). RPE thickness measurements were made at 300 μm intervals along the length of the epithelium within a single section, excluding regions within 300 μm of the optic nerve and ora serrata. As an estimate of cellular density, counts of nuclei contained within 100 μm expanses of the RPE layer were determined in the same sections and at the same sites. Both RPE thickness and cellular density have previously been reported to vary appreciably from central to peripheral regions. Consequently, in these studies we performed statistical analyses of morphometric data on a regional as well as global basis.

For transmission electron microscopy, glutaraldehyde-fixed eyes were dissected to remove the cornea and lens, and then post-fixed in 2% osmium tetroxide in phosphate buffer. After extensive rinsing in buffer and distilled water, specimens were dehydrated and embedded in Epox 812-Araldite (Ernest F. Fullam, Latham, NY). Thin (90 nm) sections were stained with uranyl acetate and lead citrate and examined in a Philips Tecnai 10 electron microscope (FEI, Hillsboro, OR). Images were acquired using a Mega-Plus Model ES 4.0 CCD camera and processed using Photoshop. Retinal attachment, defined as an overlap of greater than 50% of the length of epithelial microvilli by photoreceptor outer segments, was determined in a single section that included both the central and peripheral parts of the eye. In practice, interdigitation of the RPE and neural retina in any particular area was found to be completely intact or essentially lost, resulting in relatively little ambiguity. Regions within 300 μm of the optic nerve and ora serrata, as well as areas exhibiting outer nuclear layer dysplasia, were excluded from analysis. The length of detached retina was divided by the total linear extent of tissue surveyed and expressed as a percentage.

Cell proliferation and cell death analysis: In order to assess the impact of *p27Kip1* deletion on cell division in the

developing RPE, DNA synthesis was examined immunocytochemically following BrdU incorporation. *p27*$^{+/-}$ and *p27*$^{-/-}$ mice were injected via an intraperitoneal route with 50 μg/g body weight of a solution of BrdU (Sigma Chemical Co., St Louis, MO) in PBS. Animals were injected twice on P7, and then sacrificed on P8. After fixation in 4% paraformaldehyde, eyecup tissues were cryoprotected in 20% sucrose in PBS, frozen in melting Freon 22 and sectioned (at 10 μm) on a cryostat. Prior to antibody labeling, sections were treated for 60 min at 37 °C with 2N HCl. Immediately following acid treatment, specimens were neutralized with 0.1M borate buffer, pH 8.5 and finally rinsed in PBS. To label cells incorporating BrdU, sections were first blocked for 1 h in 10% normal goat serum in PBS containing 1% BSA and 0.2% Triton X-100, then incubated overnight at 4 °C with monoclonal anti-BrdU (1:25 dilution; Roche, Indianapolis, IN). After several washes in PBS, bound antibody was detected by staining with goat anti-mouse IgG conjugated to DTAF (1:200 dilution; Jackson ImmunoResearch Laboratories, West Grove, PA) for 1 h at room temperature. Tissue immunofluorescence was subsequently viewed by confocal laser scanning microscopy (see below).

Cell death was assessed by TUNEL assay, using a kit and instructions provided by the manufacturer (Roche). Frozen sections of 4% paraformaldehyde-fixed eyes were permeabilized with 0.1% Triton X-100 in 0.1% sodium citrate buffer and DNA strand breaks detected in situ via incorporation of fluorescein-dUTP by exogenously-applied terminal deoxynucleotidyl transferase [21]. Evaluation of DNA labeling was carried out in the confocal microscope.

Preparation of tissue whole-mounts: In order to view all cells within the RPE layer at one time, epithelial flat-mounts were prepared. For adult eyes, we adapted a previously developed procedure for harvesting the entire tissue as a single intact sheet attached to the neural retina [22]. Briefly, enucleated eyes that had been cleaned of extraocular tissue were immersed in a solution of 2% Dispase II (neutral protease; Roche) in Dulbecco's Modified Eagle's Medium (DMEM) for 35-40 min at 37 °C. After several rinses in DMEM, eyecups were prepared by making a circumferential incision just posterior to the ora serrata and discarding the anterior segment (i.e., cornea, ciliary body and lens). Subsequent peeling of the neural retina away from these eyecups resulted in the intact epithelium partitioning with the photoreceptor layer, to which it is adherent. Tissues isolated in this way were fixed in 1% glutaraldehyde in 0.1 M phosphate buffer, pH 7.4 for 2 h and, after being rinsed in buffer, mounted RPE side-up on a glass microscope slide. To ensure that the retina lay flat, several radial cuts (5-6, depending on the size of the eye) were made in the tissue from the periphery to the optic nerve area, producing "petals". Flat-mounts were then coverslipped in ProLong Gold anti-fade reagent (Invitrogen Molecular Probes, Inc., Eugene, OR) and examined unstained in a Leitz Laborlux S microscope equipped with a 40X objective. Digital images were acquired using a Spot Insight 4 camera and software (Diagnostic Instruments, Inc, Sterling Heights, MI) and processed using Photoshop. Melanin granules in these heavily pigmented adult eyes are excluded from cell borders and from regions of the cell containing nuclei, with the result that they act as a natural contrast agent. In some cases, the neural retina was removed from non-Dispase-treated eyes, and the resulting RPE-choroid-sclera whole-mounted and labeled using fluorescent probes (see below).

For early postnatal eyes, flat-mounts were prepared from epithelium-containing posterior eyecups since, at these stages, firm retinal attachment has yet to develop. Following removal of the eye from the orbit, the cornea was punctured with a 26-gauge needle and the globe fixed by immersion in ice-cold 4% paraformaldehyde in PBS. After several rinses, a circumferential incision was made at the level of the ora serrata and radial cuts produced to aid in tissue flattening. Specimens were then mounted, sclera side down, on a black microporous nitrocellulose membrane (MicronSep; GE Osmonics, Minnetonka, MN) and each of the "petals" gently pressed in contact with the membrane. The underside of the membrane was subsequently blotted onto a piece of dry filter paper (Whatman, Florham Park, NJ) to wick away excess fluid and encourage the tissue to flatten completely. To expose the RPE layer, another piece of membrane was carefully placed atop the vitreal surface of the retina, allowed to adhere and then peeled away. In most cases, the neural retina separated cleanly from the epithelium, permitting direct access to the latter's apical surface. Occasionally, separation took place between the RPE and choroid, with the epithelium coming off as a sheet with the membrane-attached neural retina. This allowed the RPE layer to be viewed from its basal aspect.

To visualize the boundaries of individual RPE cells in adult or early postnatal eyes, flat-mounts were stained with Alexa Fluor 488-phalloidin (5 U/ml in TBS, containing 1% BSA and 0.2% Triton X-100) for 30 min at room temperature. Fluorescent phalloidin binds to polymerized actin filaments, which exist as a circumferential bundle encircling cells at the apical end of their lateral borders. Consequently, labeling is readily visualized as a polygon that completely outlines the cell at the level of cell-cell junctions and allows counts of cell number to be made. After several TBS rinses, flat-mounts were placed on glass slides with the epithelium facing up and mounted in Vectashield fluorescence mounting medium (Vector Labs, Burlingame, CA). In certain cases, nuclear staining was additionally carried out by exposure to propidium iodide (0.1 mg/ml in TBS, containing 0.5 mg/ml RNAase A; Roche) or To-Pro-3 (2 mM in PBS; Molecular Probes), also for 30 min. However, in order to view propidium iodide-labeled nuclei unobstructed by the high density of melanin present in the apical RPE of this mouse strain, it was necessary to obtain images from the basal aspect of the epithelium following its partitioning with the peeled neural retina. Ultimately, specimens were viewed in a Leica SP confocal laser scanning microscope (Leica, Heidelberg, Germany) equipped with a 20X infinity-adjusted objective. A series of 1 μm-thick optical sections was obtained through the z-axis of the specimen and used to construct an extended focus image consisting of all optical sections in the data set. All micrographs presented consist of a stack of seven to ten serial sections, except where

otherwise indicated. In all cases, wild-type and mutant specimens were processed in the same manner and images were acquired using identical instrumental parameters. Counts of cellular and nuclear density in flat-mounts, including those that were left unstained and those labeled with fluorescent probes, were performed by multiple sampling of epithelial regions midway between the optic nerve head and the ora serrata and normalizing the results to a unit area of 50,000 mm^2.

Statistical analysis: Data are reported as the mean±SEM, using only one eye from an individual animal for any quantitative assay. Each number is, in turn, representative of the numerical average of multiple measurements made within a particular tissue specimen. Statistical comparisons between experimental groups were conducted using either Student's t-test or one-way ANOVA (SYSTAT, SPSS, Chicago, IL), followed by Fisher's LSD multiple range test of significance. The Pearson product moment correlation coefficient, r, was calculated using Excel (Microsoft, Redmond, WA).

RESULTS

Epithelial overproliferation in $p27^{Kip1}$*-null retinas:* In 5 week-old mice, the mutant RPE is appreciably larger in its apical to basal dimension than corresponding tissues from animals of the other two genotypes (Figure 1A,B,C; compare insets). Analysis of the average thickness of the epithelial layer in transverse sections from the three sets of mice show that the nullizygous RPE is approximately 6% thicker than the hemizygous RPE and 12% thicker than the wild-type RPE (Figure 2A). This change occurs uniformly throughout the retina and is not restricted to retinal regions exhibiting outer nuclear layer dysplasia: epithelial thickness averages 5.34±0.11 and 5.38±0.11 for non-dysplastic and dysplastic areas of mutant retinas, respectively.

In addition to being thicker, the mutant epithelium also appears in light micrographs to contain more nuclei per field of view (Figure 1A,B,C; compare insets). When measurements of the linear packing density of nuclei are made in plastic sections, as an indirect estimate of cell number, there is a 63 and 96% increase in the number of nuclei per unit length in the nullizygous RPE, compared with the hemizygous and wild-type RPE, respectively (Figure 2B). As with epithelial thickness, a comparable increase is seen in all parts of the retina, including both central and peripheral regions, and appears to be uncorrelated with areas of retinal dysplasia.

In order to test whether the increased nuclear packing density in the mutant RPE reflects increased cellular density, unstained epithelial layers were visualized as flat-mounts. Fig-

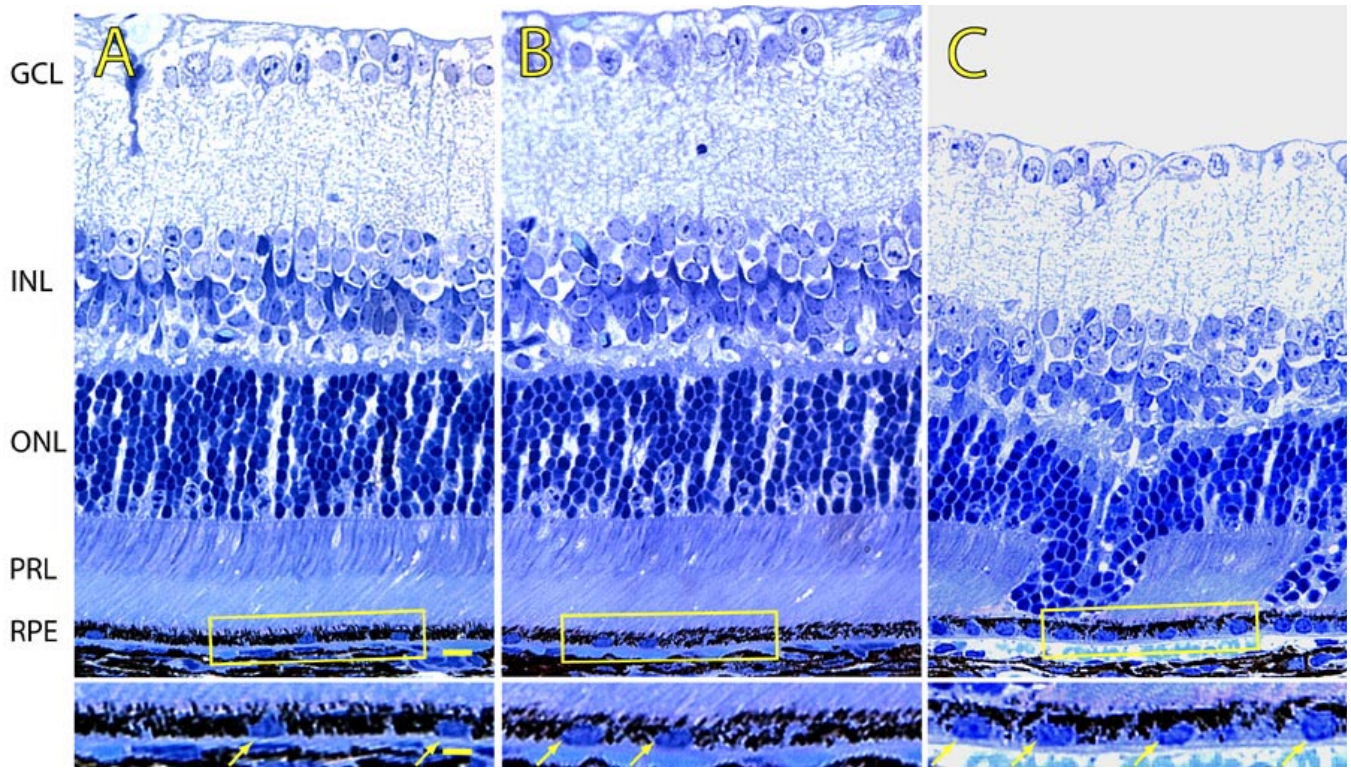

Figure 1. Light micrographs of JB-4 retinal sections derived from 5 week-old wild-type and $p27^{Kip1}$ hemizygous and nullizygous mice. **A** represents $p27^{+/+}$, **B** represents $p27^{+/-}$, and **C** represents $p27^{-/-}$ retinal tissue. The RPE cell layer from $p27^{Kip1}$-null animals appears thicker, with increased numbers of nuclei (arrows in insets). Also, in the mutant retina melanin granules tend to occupy more apical portions of the cytoplasm. Note that the dysplasia of the outer nuclear and photoreceptor layers is evident in the $p27^{Kip1}$-null retina only. RPE represents retinal pigment epithelium; PRL represents photoreceptor layer; ONL represents outer nuclear layer; INL represents inner nuclear layer; GCL represents ganglion cell layer. Scale bar represents 10 μm. Inset scale bar represents 20 μm.

ure 3 compares images obtained from preparations of wild-type and mutant retinas. The RPE monolayer from normal animals is comprised of a relatively uniform array of cells that are polygonal in shape, containing a mixture of mainly mononucleated and binucleated cells (Figure 3A). While similar in overall arrangement, the nullizygous epithelium appears more crowded, with cells that are generally smaller in diameter (Figure 3B,C,D). In addition, mutant epithelia are sometimes observed to contain more cells with nuclei displaced from their usual central position to the periphery (Figure 3D). We also examined the RPE actin cytoskeleton in flat-mounted tissues after staining with Alexa Fluor 488-phalloidin. Wild-type monolayers display highly regular arrays of microfilaments in the form of rings that define the apical boundaries of individual epithelial cells (Figure 3E). These circumferential microfilament arrays are also present in mutant cells; however they are much reduced in diameter and vary in their apical-basal localization (Figure 3F).

Cellular and nuclear density measurements were made on images similar to those shown in Figure 3A-D and the results plotted graphically. As seen in Figure 4A, there are approximately twice as many nuclei per unit area in the nullizygous epithelium, compared to that of the wild-type. Surprisingly, this rather large change in nuclear density is accompanied by a smaller increase (46%) in cellular density. Such results are indicative of an alteration in the overall ratio of uninucleated to multinucleated cells, and this is demonstrated in Figure 4B. Whereas the normal RPE consists, on average, of 46% binucleated cells, the comparable figure in mutants is 89%.

We also examined RPE monolayers from early postnatal time points in order to monitor proliferative changes developmentally. Figure 5 shows full thickness confocal scans through flat-mounts of P7 wild-type and mutant epithelia that have been stained with Alexa Fluor 488-phalloidin and propidium iodide to label cell boundaries and nuclei, respectively. Clear differences in cellular and nuclear density are apparent even at this relatively early stage, prior to photoreceptor outer segment development and the dysplastic changes that arise in the neural retina. Measurements indicate that there is a 100% increase in nuclear density in the nullizygous RPE, compared with the wild-type tissue (Figure 6). As with the adult epithelium, this is accompanied by a significantly smaller increase (39%) in cellular density. Quantitatively similar increases are observed for P0 mutant epithelia, at a time when most wild-type RPE cells are mononucleated [23] (data not shown). Unfortunately, the presence of light-absorbing melanin pigment precluded simultaneous visualization of individual cells and their nuclei in fluorescence images of these early time points. Consequently, the impact of gene deletion on the relative numbers of mononucleated and binucleated cells could not be assessed.

In principle, the increases seen in nuclear and cellular density in the mutant RPE could be the result of either augmented cell division, diminished cell death, or both. To obtain direct evidence for enhanced mitotic activity in the nullizygous epithelium, a BrdU incorporation experiment was carried out. $p27^{+/-}$ and $p27^{-/-}$ mice were injected twice on P7 and their retinas analyzed for uptake of the analog into DNA one day later by immunocytochemistry. At this time, very few, if any, BrdU-positive cells are seen in the hemizygous RPE or neural retina (Figure 7A). By contrast, in mutants both the epithelium and developing outer and inner nuclear layers of the retina contain examples of BrdU-positive cells (Figure 7B). In addition to proliferative changes, we also looked for differences in the relative numbers of dying cells in the RPE from hemizygous and nullizygous animals at P8 using the TUNEL assay. As seen in Figure 7C,D, there is little evidence for apoptosis in the RPE of either genotype, although TUNEL-positive cells can be seen in the neural retinas of normal animals and are abundant in mutants.

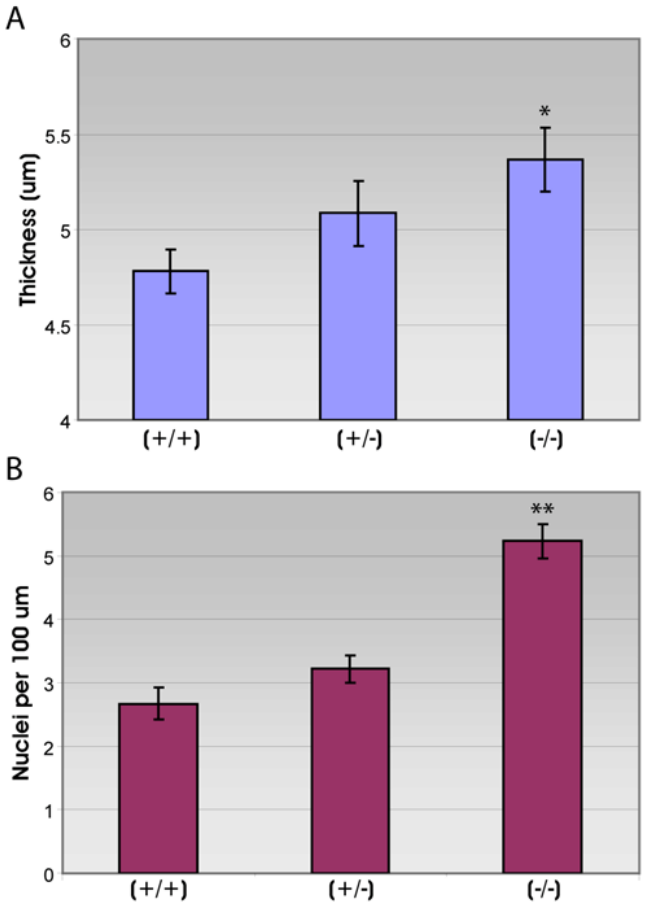

Figure 2. Retinal pigment epithelium thickness and nuclei per unit length in retinal sections from wild-type and $p27^{Kip1}$ hemizygous and nullizygous mice. Measurements of retinal pigment epithelium (RPE) thickness (**A**) and nuclear density (**B**) were performed on JB-4 sections from retinas of 5 week-old $p27^{+/+}$, $p27^{+/-}$ and $p27^{-/-}$ mice. The apical to basal dimension of the $p27^{Kip1}$-null epithelium is, on average, approximately 6 and 12% greater than that of the hemizygous and wild-type tissues, respectively. There is also a nearly 2 fold increase in the density of nuclei for "knock-out" animals, relative to the other two genotypes (Graph of means±SEM for 5 replicates in each condition). Asterisk (*) indicates $p<0.02$ and double asterisks (**) indicates $p<0.001$ compared to wild-type.

The differential impact that loss of *p27^{Kip1}* has on nuclear and cellular density of the RPE could be cell type-specific. To investigate this, we also examined the corneal endothelium, a tissue that displays a quantitatively similar increase in nuclear density in *p27^{Kip1}*-null mice [24]. Figure 8 compares flat-mounted endothelial monolayers from adult *p27$^{+/+}$* and *p27$^{-/-}$* mice that have been stained with Alexa Fluor 488-phalloidin and To-Pro-3. While a significantly greater nuclear density is seen in the mutant endothelium, this is matched by a comparable change in cellular density. Thus, unlike the case with the RPE, loss of *p27^{Kip1}* results in a corneal endothelium possessing increased numbers of mononucleated cells only.

Retinal attachment in wild-type versus p27^{Kip1}*-null retinas:* It is normally relatively difficult to separate the neural retina from the RPE of adult wild-type mice by peeling without causing damage to epithelial cells [25,26]. However, in our studies examining RPE proliferation, we noticed a decline in the apparent adhesiveness of nullizygous retinas. Figure 9A shows representative examples of neural retinas that were peeled from *p27$^{+/-}$* and *p27$^{-/-}$* eyecups 3 h after light onset. In the hemizygous retina, abundant melanin pigment decorates the photoreceptor surface more or less uniformly (Figure 9A). Higher power views of the flat-mounted tissue demonstrate that this pigment is contained mainly in epithelial microvilli

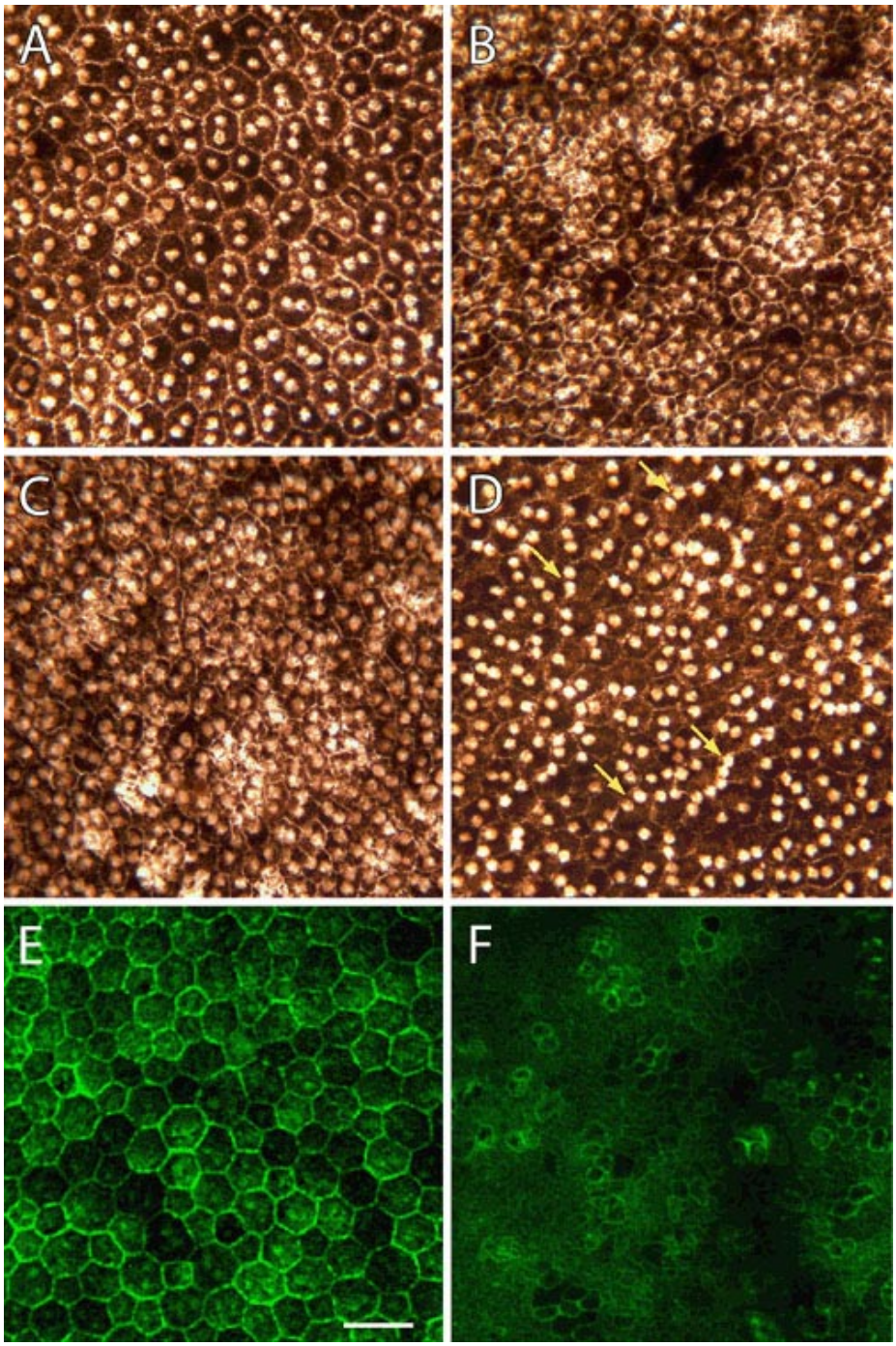

Figure 3. Flat-mounts of wild-type and mutant retinal pigment epithelium from P35 retinas. Whole-mounted retinal pigment epithelium (RPE) tissue from wild-type (**A** and **E**) and mutant (**B**, **C**, **D**, and **F**) P35 retinas were left unstained (**A**-**F**) or labeled with Alexa Fluor 488-phalloidin (**E** and **F**). In unstained preparations, the normal epithelium consists of relatively uniform polygonal cells with centrally-located nuclei (**A**). Mutant cells are, by contrast, smaller in diameter and less regular in their outline. While cellular density can vary somewhat, regions of the nullizygous RPE exhibiting a higher nuclear density also display increased cellular density (compare **B**, **C**, and **D**). In some mutant eyes, there are increased numbers of epithelial cells with nuclei displaced from central to peripheral regions (**D**, arrows). In 1 μm thick optical sections of Alexa Fluor 488-phalloidin-labeled tissues, apical cell boundaries are marked by rings of actin filaments associated with intercellular junctions, while microvillous processes are evident as punctate dots overlying the cytoplasm (**E** and **F**). Note the alignment and regularity of cell outlines in the wild-type RPE layer (**E**). The cytoskeleton of mutant epithelial cells, on the other hand, appears less well organized, and Alexa Fluor 488-phalloidin staining defines apical membrane compartments that are much smaller and more variable in diameter (**F**). Scale bar represents 40 μm.

and portions of the apical cell cytoplasm that have been sheared from cells during mechanical separation (Figure 9B), a reflection of the strong physical interaction between the two tissues. The nullizygous retina, on the other hand, retains relatively little melanin, which is suggestive of a much weaker adhesion to the RPE layer (Figure 9A,C).

To assess whether the difference in apparent retinal adhesiveness that we observe has a structural basis, wild-type and mutant ocular tissues were examined in semi-thin and thin plastic sections. As seen in Figure 10A,C, the RPE and neural retina of normal mice are closely apposed, with rod photoreceptors directly abutting the apical epithelial surface. Furthermore, electron microscopic images demonstrate that individual outer segments are ensheathed by RPE microvillous processes, which are generally seen to extend more than 20 μm along the length of outer segments (Figure 10F). Retinas from *p27^{Kip1}*-null animals, on the other hand, oftentimes display irregular gaps between the apical surface of the epithelium and rod tips (Figure 10B). When viewed at higher power, these gaps are seen to be regions where the tissue interface is disrupted by a partial or complete separation between the two cell layers (Figure 10E). Furthermore, in such detached regions the RPE microvillar length appears to be significantly reduced (Figure 10G). While separation between the mutant RPE and neural retina sometimes takes place in zones of outer nuclear layer dysplasia, it is certainly not limited to these areas. Conversely, normal cellular relationships are oftentimes preserved in the vicinity of dysplastic regions, even where displaced photoreceptor cell bodies are found at the RPE surface (Figure 10D).

We have quantified retinal detachment by determining the percentage of the neural retina exhibiting close interdigitation of epithelial microvilli and photoreceptor outer segments. In each of the wild-type retinas examined, there is complete overlap between the two cell types in the entire sampled region, from the ora serrata to the area of the optic nerve (Figure 11). On the other hand, the extent of detachment in mutant retinas is substantial, averaging 42%. However, because this detachment varies considerably from eye to eye (range: 5 to 81%), we considered the possibility that RPE-neural retina separation might be a function of the amount of outer nuclear layer dysplasia present. The latter also exhibits wide deviation, involving anywhere from 1 to 16% of the tissue in any one retinal section (average: 8%). Consequently, in expressing the extent of RPE-photoreceptor interaction quantitatively we plotted percentage detachment as a function of percentage dysplasia. As shown in Figure 11, our results indicate that there appears to be little correlation between outer nuclear layer dysplasia and the magnitude of retinal detachment.

In view of the substantial changes observed at the RPE-neural retina boundary, it is surprising that epithelial cells from wild-type and nullizygous animals are generally similar in their overall ultrastructural characteristics (Figure 10C-G). Nevertheless, we occasionally observe examples of what appear to be incompletely or abnormally polarized RPE cells (Figure 12). Such cells exhibit microvillar inclusions, areas where microvillous processes are found in vacuoles within the cell cytoplasm rather than on its surface. More commonly, however, regions are seen where basal infoldings appear to extend into and invade the lateral membrane interface between cells within a monolayer. While both types of abnormality are relatively rare, they are virtually never observed in the wild-type epithelium.

DISCUSSION

In this study we have presented evidence that p27^{Kip1} plays an important role in regulating RPE mitosis during retinal histogenesis. Mice with targeted deletion of the *p27^{Kip1}* gene exhibited a higher density of nuclei in their epithelial monolayers, compared with wild-type and hemizygous controls. This dif-

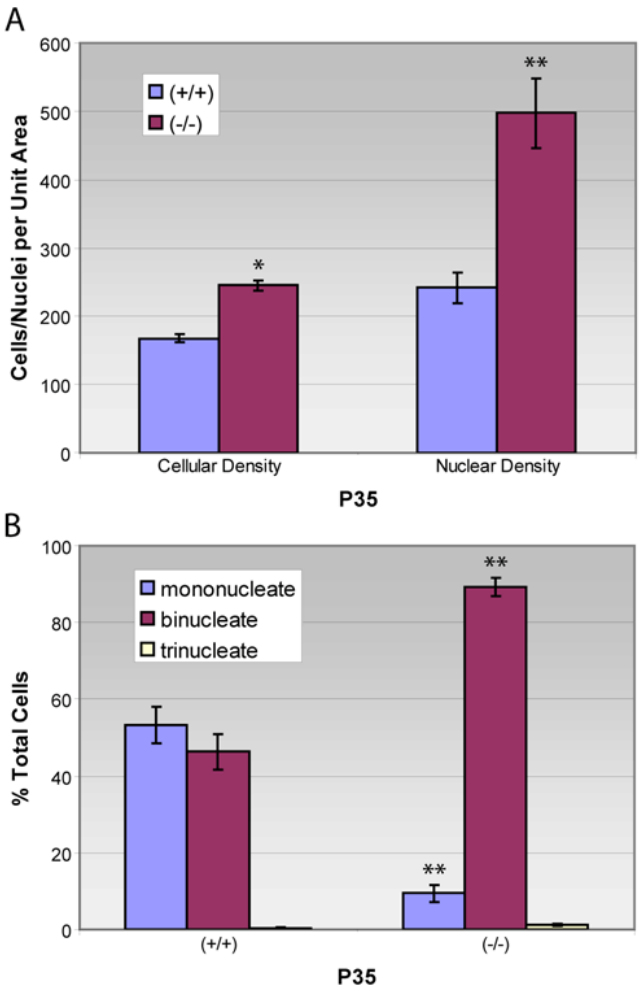

Figure 4. Cellular and nuclear density and number of nuclei per cell in retinal pigment epithelium from 5 week-old wild-type and mutant mice. Measurements of (**A**) cellular and nuclear density and (**B**) percent uninucleated versus multinucleated cells were made using unstained flat-mounted tissues from *p27$^{+/+}$* and *p27$^{-/-}$* animals as depicted in Figure 3 and counts normalized to an area of 50,000 mm^2. Compared with wild-type tissues, the mutant epithelium exhibits a 100% increase in nuclear density, but only a 46% increase in cellular density. Consequently, mutant RPE cells contain a higher proportion of multinucleated cells (Graph of means±SEM for 7 replicates in each condition). Asterisk (*) indicates p<0.01 and double asterisks (**) indicates p<0.001 compared to wild-type.

ference, approximately 2 fold, was evident even at early postnatal ages and likely reflects the generation of ectopic nuclei beginning with the embryonic period. Our previous work examining p27^{Kip1} expression by rodent RPE has indicated that the protein is upregulated at mid to late gestational periods and is maximal around birth [27]. Thus, the data we have obtained are consistent with the possibility that this negative cell cycle regulator normally acts to influence cell cycle duration, or to control the proportion of cells that exit the cell cycle, during specific developmental intervals [28]. Recently, Yoshida et al. [29] presented results of nuclear counts performed on the RPE of adult *p27^{Kip1}*-null mice, yielding data that are quantitatively very similar to ours. Furthermore, these authors also reported that the mutant RPE incorporated BrdU during postnatal days 7 through 10, at a time when the normal epithelium is quiescent. In addition to confirming this finding, we have presented data indicating that naturally-occurring cell death is unlikely to play a significant role in the proliferative response seen in RPE cells of mutant animals. In this respect, the developing epithelium reacts very differently to *p27^{Kip1}* gene ablation than the neural retina, which largely deletes an initial overproduction of cells through apoptosis [17,18]. Overall, the combined evidence indicates that the RPE of *p27^{Kip1}*-null mice undergoes, on average, at least one additional round of

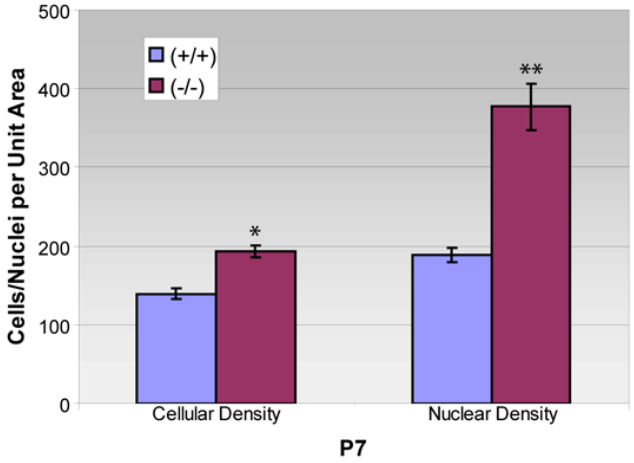

Figure 6. Cellular and nuclear density of retinal pigment epithelium from P7 wild-type and mutant mice. Measurements of epithelial cellular and nuclear density were made using flat-mounted tissues from *p27$^{+/+}$* and *p27$^{-/-}$* animals, after being stained as depicted in Figure 5. Compared with wild-type tissues, the mutant epithelium exhibits a 100% increase in nuclear density, but only a 39% increase in cellular density (Graph of means±SEM for 3-5 replicates in each condition). Asterisk (*) indicates p=0.001 and double asterisks (**) indicates p<0.005 compared to wild-type.

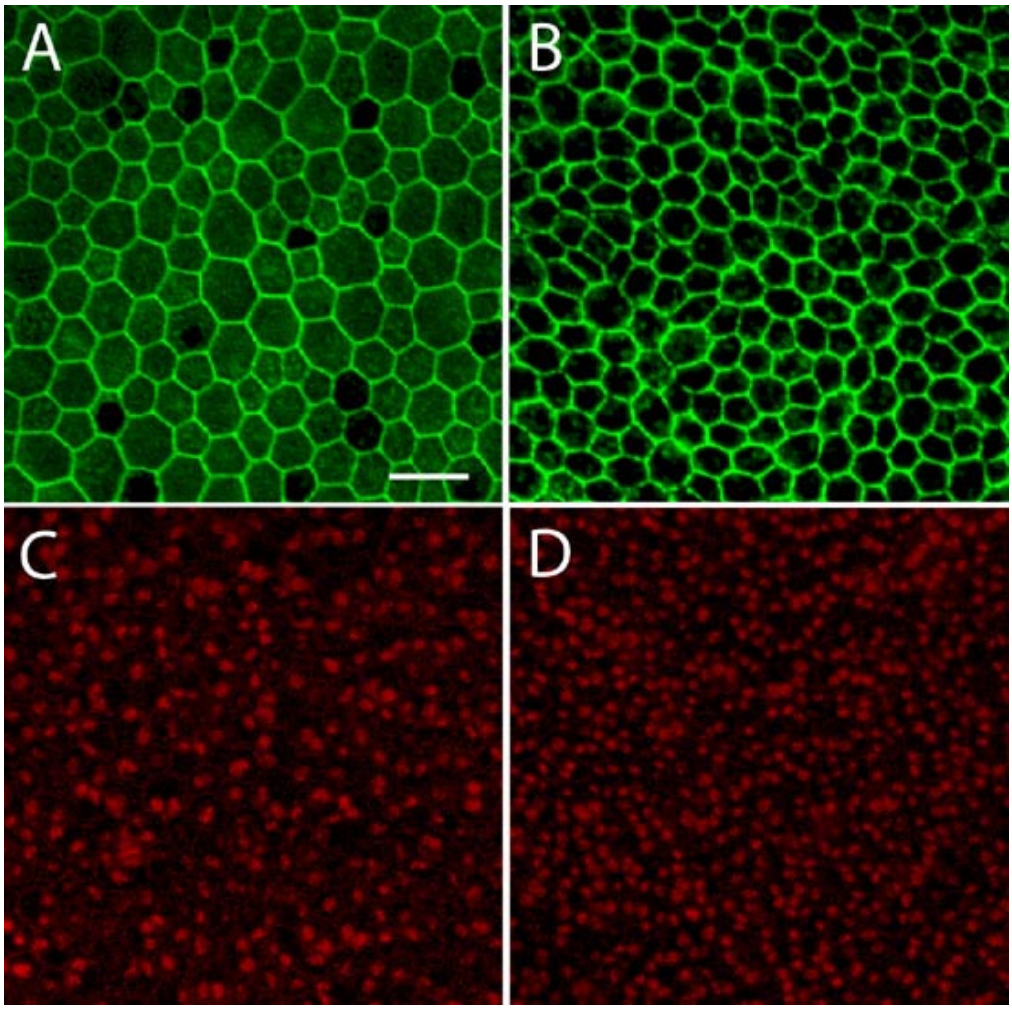

Figure 5. Flat-mounts of wild-type and mutant retinal pigment epithelium from P7 retinas. Whole-mounted retinal pigment epithelium (RPE) tissue from wild-type (**A** and **C**) and mutant (**B** and **D**) P7 retinas were labeled with Alexa Fluor 488-phalloidin (**A** and **B**) and propidium iodide (C and D) and examined by confocal microscopy. An increase in cellular and nuclear packing density is apparent in these images taken from a region midway between the central and peripheral retina. Scale bar represents 40 μm.

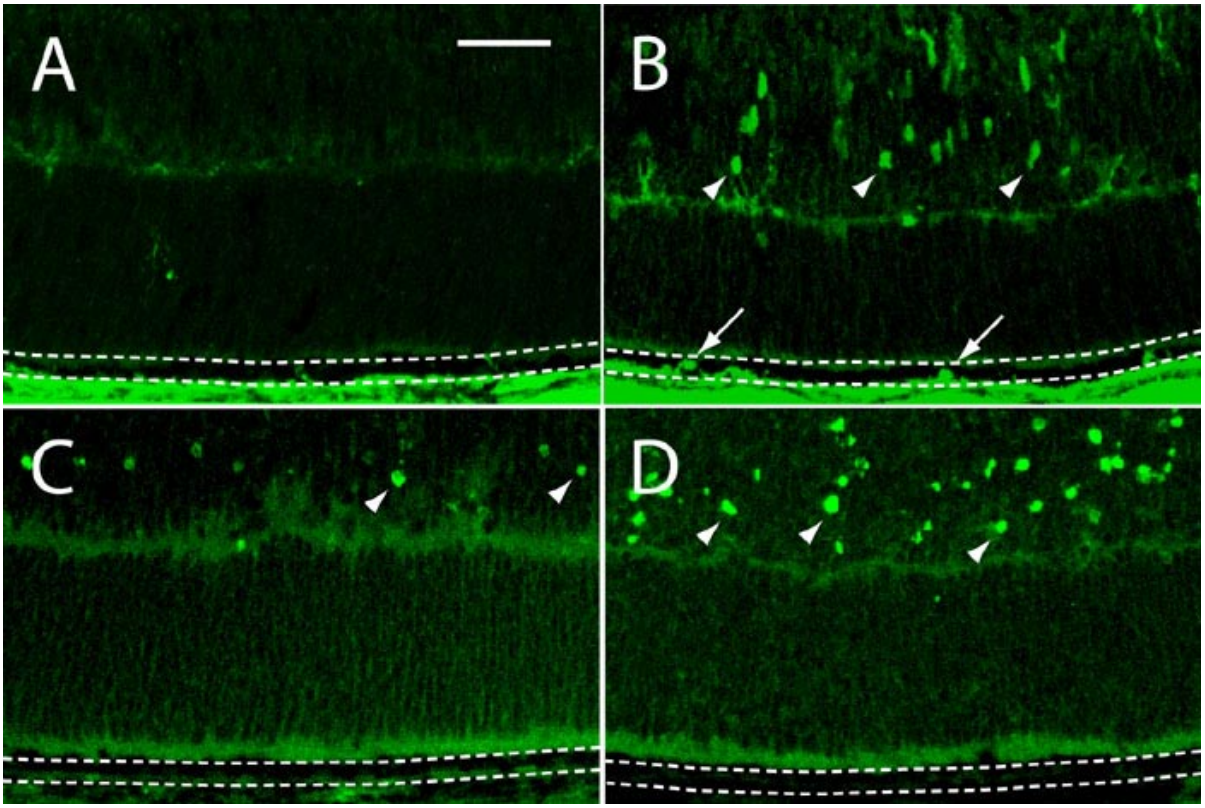

Figure 7. Cell proliferation and cell death in frozen sections of retinas from developing *p27^{Kip1}* hemizygous and nullizygous mice. **A** and **C** represent *p27$^{+/-}$* and **B** and **D** represent *p27$^{-/-}$* tissues. **A** and **B**: BrdU incorporation. Representative photomicrographs of the peripheral retina from animals injected on P7 and sacrificed on P8. Immunoreactive nuclei (arrows) are present in the nullizygous (**B**), but not hemizygous (**A**), RPE (between dotted lines). Note also the presence of BrdU-positive cells in the developing inner nuclear layer of the mutant retina (arrowheads). **C** and **D**: TUNEL assay. Apoptotic epithelial cells are undetectable in P8 retinal sections from both genotypes. On the other hand, TUNEL-positive cells are seen in the hemizygous neural retina and are especially plentiful in the nullizygous neural retina (arrowheads). Scale bar represents 40 μm.

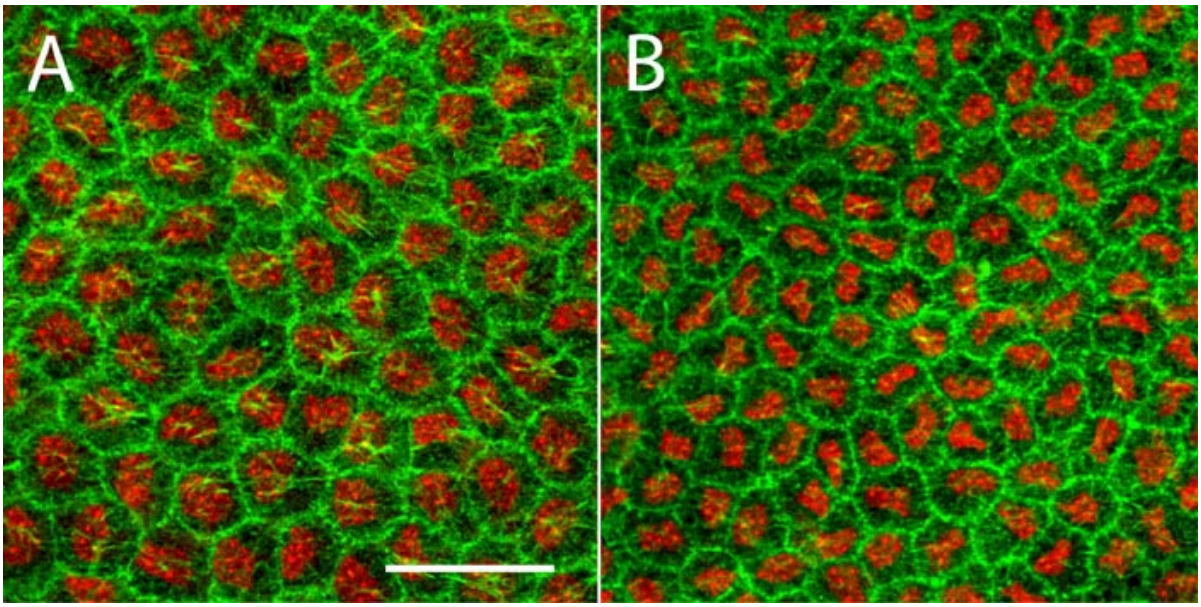

Figure 8. Flat mounts of wild-type and mutant corneal endothelium from P35 eyes. Whole-mounted corneas from *p27$^{+/+}$* and *p27$^{-/-}$* mice were stained with Alexa Fluor 488-phalloidin and ToPro-3 and examined by confocal microscopy. As is apparent from these projection images, the mutant endothelium consists of an ordered array of cells with an appreciably higher density than that of the normal tissue. Nevertheless, both monolayers possess predominantly, if not exclusively, mononucleated cells. Scale bar represents 40 μm.

mitosis during the period of normal cell generation. Both altered cell cycle dynamics and a delay in the timing of cell cycle withdrawal could be contributing to the enhanced nuclear density seen in *p27*$^{-/-}$ monolayers.

An interesting feature of rodent RPE is the fact that a substantial percentage of cells is normally multinucleated [23,30]. Thus, the increased mitoses observed in *p27*^{Kip1} "knock-out" mice could, theoretically, result in the generation of either more total cells or more cells with multiple nuclei. The data we have obtained from adult animals clearly show that both mechanisms take place. Roughly half of the enhancement in RPE nuclear density can be accounted for by cell division, while the other half is likely due to the conversion of mononucleated to binucleated cells. The fact that *p27*^{Kip1} mutant epithelia from neonatal animals show a similar disparity in nuclear and cellular density increases suggests that, during relatively early times, mitosis and cytokinesis are partially uncoupled from one another. Whether this reflects an incomplete block in epithelial cell division as a result of checkpoint controls is not clear. However, it is well-established that a final wave of acytokinetic mitosis is a normal feature of rodent RPE cell proliferation during the first week of postnatal development [30]. Thus, the enhanced numbers of binucleated cells seen in mutants may reflect cell division mechanisms inherent to the epithelium that are self-limiting. In any event, our results demonstrate that this phenomenon cannot be generalized to other tissues, since ectopic cells generated by the corneal endothelium of *p27*^{Kip1}-null animals consist almost exclusively of those with single nuclei.

It has previously been reported by others that mutant RPE cells from adult *p27*^{Kip1}-null animals appear taller than those of their normal litter mates [16]. Using morphometric analysis, we have been able to confirm this observation quantitatively. Our results indicate that the nullizygous RPE is approximately 12% thicker, in its apical to basal dimension, than that of the wild-type epithelium. Importantly, while monolayers from these mutant animals exhibited a higher cellular density they appeared normal, with little evidence for multilayering

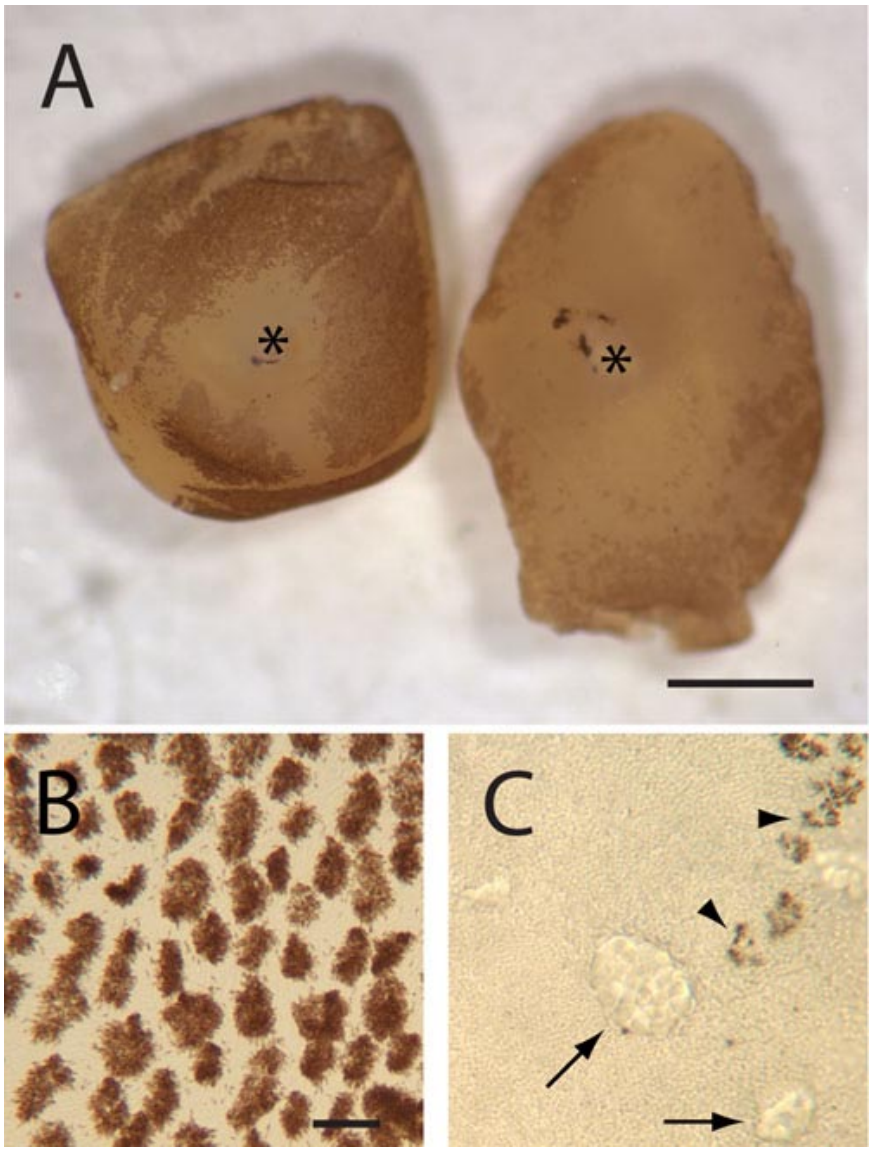

Figure 9. Neural retinas peeled from the eyes of 5 week-old *p27*$^{+/-}$ and *p27*$^{-/-}$ mice. **A**: Stereomicroscope view. Melanin pigment granules (dark brown) cover much of the outer surface of the hemizygous retina (left), except in the area surrounding the optic nerve (*). By contrast, the peeled nullizygous retina has relatively little adherent pigment in central regions, although some melanin is present in more peripheral regions (right). **B** and **C**: Bright-field micrographs. To obtain these images, the same retinas as seen in (**A**) were flat-mounted and typical regions viewed at high power. Melanin granule-containing microvillous processes (arrowheads in **C**), which have broken off during tissue separation, are present in much larger numbers in the hemizygous, as compared to the nullizygous, retina. Arrows indicate regions of outer nuclear layer dysplasia. **A**: Scale bar represents 1 μm. **B** and **C**: Scale bar represents 20 μm.

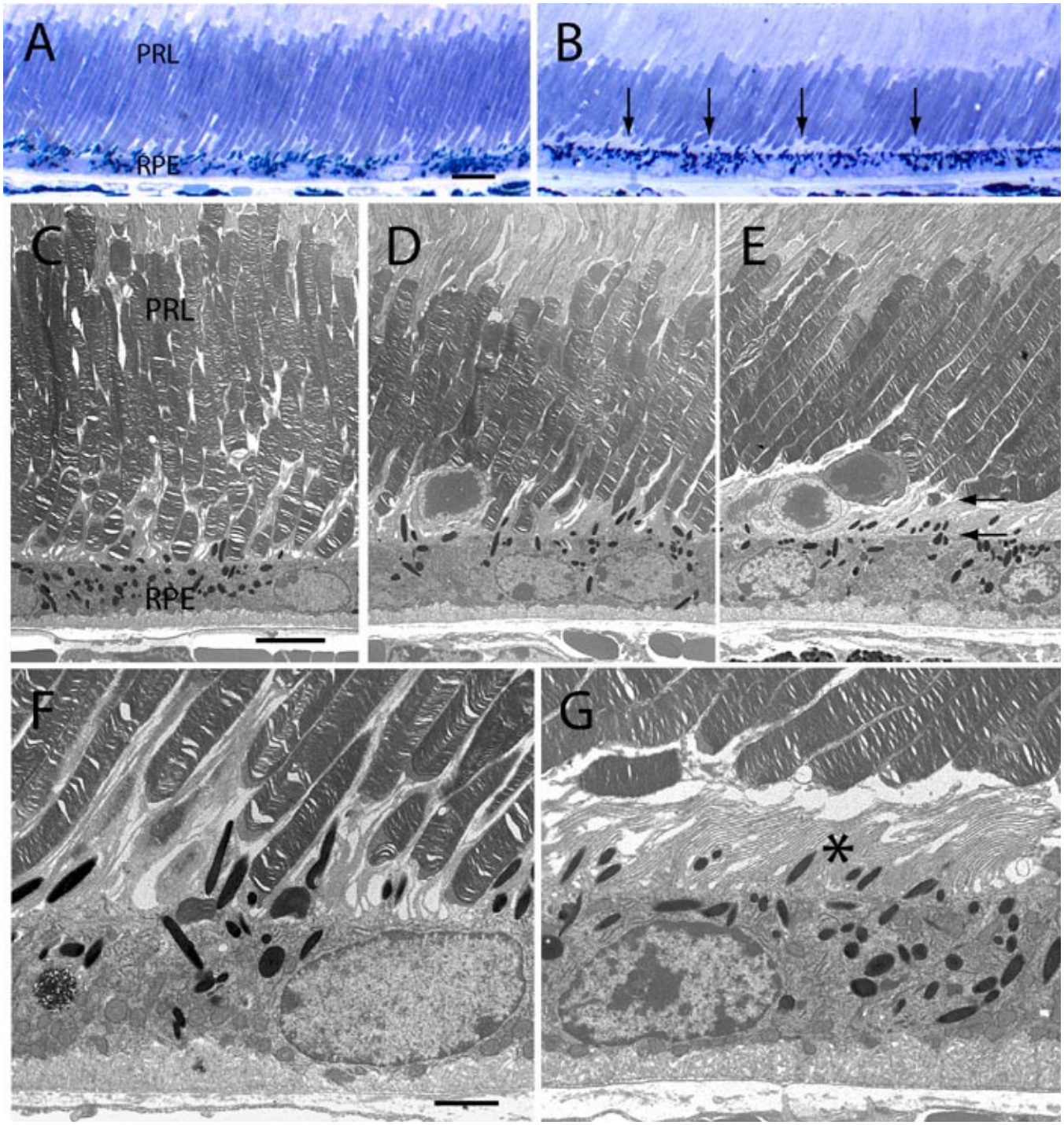

Figure 10. Light and electron micrographs of the RPE-neural retina boundary from 5 week-old wild-type and *p27^{Kip1}*-null mice. **A**, **C**, and **F** represents *p27$^{+/+}$* and **B**, **D**, **E**, and **G** represents *p27$^{-/-}$* retinal tissue. Comparison of images from semi-thin sections reveal that, while the RPE and neural retina of normal eyes are contiguous (**A**), variable-sized gaps appear between these two tissues in mutant eyes (**B**, arrows). In electron micrographs, direct contact is seen between the tips of rod photoreceptors and the apical epithelial surface both in the normal retina (**C**), and in some regions of the mutant retina (**D**). However, in other regions of the mutant retina, these two cell types are often separated from one another by a variable space (between arrows in **E**). In such regions, epithelial microvillous processes are often seen to lose their normal close interdigitation with rod outer segments. This results in a partial or complete separation of RPE and neural retina at their boundary, with the intervening space taken up largely by microvilli (asterisk in **G**). Although displaced rod nuclei are occasionally observed at the mutant RPE-neural retina interface, most outer segments appear structurally normal. Furthermore, the morphology of the epithelial cell layer in thin sections is generally comparable in the two types of animals. RPE represents retinal pigment epithelium; PRL represents photoreceptor layer. **A** and **B**: Scale bar represents 10 μm. **C**, **D**, and **E**: Scale bar represents 5 μm. **F** and **G**: Scale bar represents 2 μm.

at any time point. Thus, the increased thickness of the epithelium may, at least partially, be accounted for by an apical to basal expansion of individual cells as a result of cell crowding. On the other hand, RPE cells from *p27*^{Kip1}-null mice generally appear much smaller in diameter that their wild-type litter mates. This suggests that, concomitant with an enhancement in cellular density, the average size of individual epithelial cells decreases considerably, notwithstanding the relatively small increase in epithelial thickness. Such an alteration in average cell volume might be indicative of a mechanism whereby cells adjust their rate of growth or enlargement in order to conform to a defined tissue size.

An unexpected finding of this report is the fact that *p27*^{Kip1} gene ablation leads to both a decline in apparent retinal adhesiveness and a disruption of normal retinal attachment, the latter being evident as either a partial or complete loss of RPE-photoreceptor interdigitation. It's possible that these defects are related to the enhanced proliferative response seen in the epithelium. However, our data show that, while a near maximal RPE mitotic response is established early in postnatal development, the overall architecture of the epithelium and the arrangement of its actin cytoskeleton appear normal at this stage. In this regard, it is interesting that an upregulation of

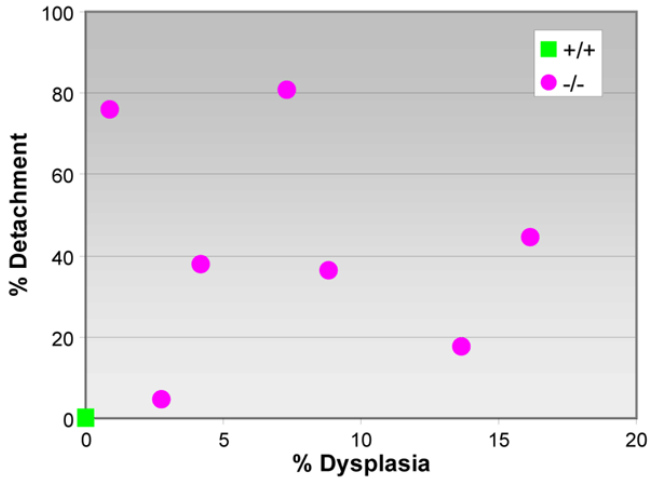

Figure 11. Measurements of percentage retinal detachment and outer nuclear layer dysplasia in electron micrographs from 5 week-old *p27*$^{+/+}$ and *p27*$^{-/-}$ mice. In each of the wild-type retinas examined, there is virtually no evidence of either detachment or dysplasia (n=4). Mutant retinas, on the other hand, exhibit both types of structural abnormality in varying amounts. However, loss of RPE-photoreceptor interdigitation appears to be uncorrelated with the magnitude of outer nuclear layer dysplasia (r=-0.189).

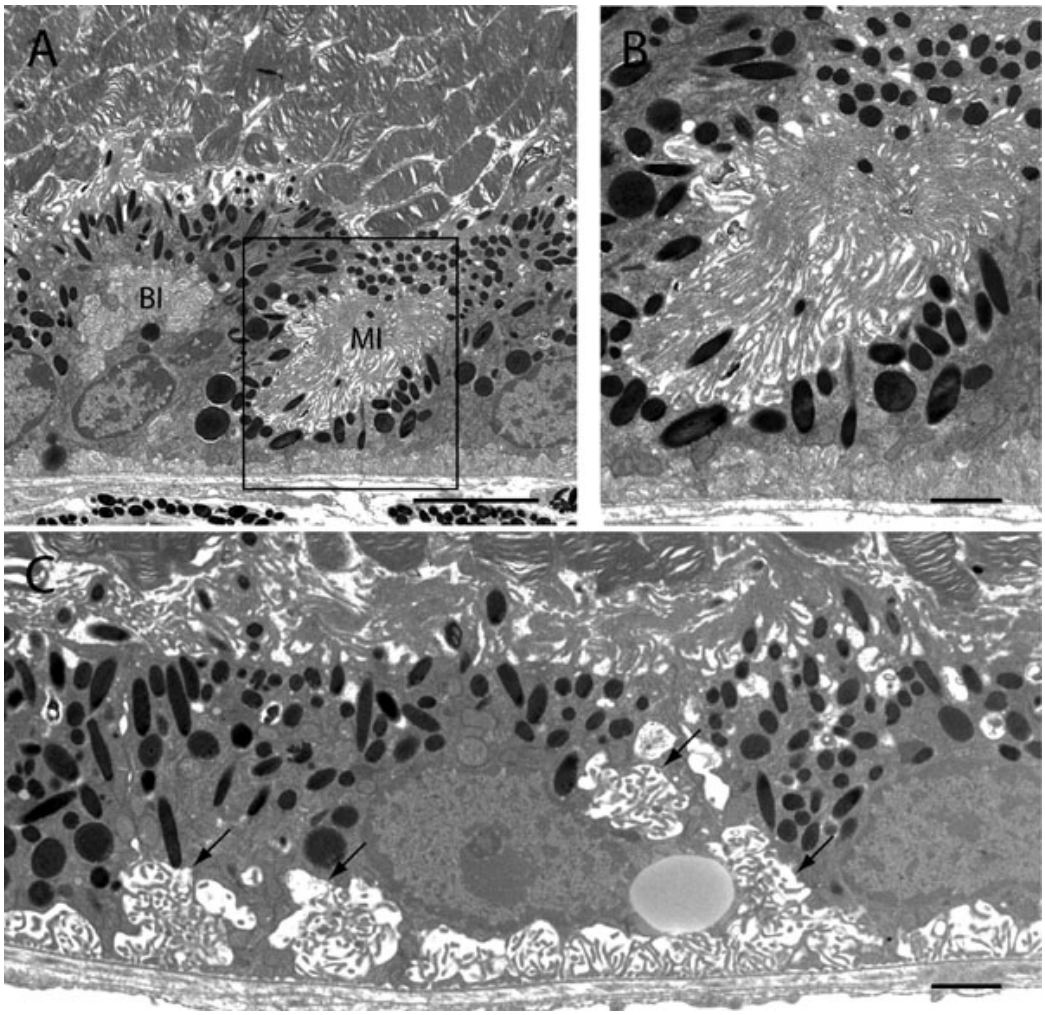

Figure 12. Electron micrographs of the RPE-photoreceptor interface from a *p27*^{Kip1}-null retina. The low power image (**A**) shows an incompletely polarized epithelial cell displaying a microvillar inclusion (MI), as well as an inclusion of basolateral membrane (BI), within the cytoplasm of the cell. The boxed region in **A** is seen at higher power in **B**. The micrograph shown in **C** represents a region where there is an apparent expansion of the basal surface membrane, which also tends to occupy more central and lateral portions of cells (arrows). Such polarization defects occur in well-oriented regions of the retina. **A**: Scale bar represents 5 μm. **B**: Scale bar represents 1 μm. **C**: Scale bar represents 2 μm.

p27^{Kip1} has been reported following experimental retinal detachment in mice [31].

Another candidate process that could be influencing RPE-photoreceptor interdigitation is the dysplasia that characterizes limited portions of the mutant neural retina. These dysplastic areas represent regions where the outer limiting membrane has been disrupted as a result of Müller cell activation and reactive gliosis, and are associated with areas of photoreceptor loss [17,18]. However, we have been unable to obtain evidence for a correlation between the magnitude of outer nuclear layer dysplasia and retinal detachment. Furthermore, loss of RPE-photoreceptor interdigitation, unlike the focal areas of dysplasia, occurs more or less uniformly throughout the retina. Nevertheless, we cannot exclude the possibility that structural alterations in the neural retina are responsible for the detachment we see.

The adult *p27^{Kip1}*-deficient RPE, while generally indistinguishable ultrastructurally from the wild-type epithelium, displays a number of alterations in cell surface specializations that are limited in their extent. For example, in areas of retinal detachment, there is oftentimes a shortening of apical microvillous processes. Less commonly, we have also seen what appear to be deformations or expansions of the basolateral plasma membrane and, on rare occasions, examples of incompletely polarized cells. The latter are characterized by microvillar inclusions, areas where microvillous processes are found in vacuoles within the boundaries of the cytoplasm rather than on the cell surface. This peculiar morphology has been observed in intestinal epithelial cells from patients with microvillous inclusion disease [32], as well as in epithelial cell lines cultured in low Ca^{++}-containing media [33]. Interestingly, similar structures have very recently been found in the native RPE of mice with targeted deletion of the ezrin gene [34]. Thus, a number of potential cytoskeletal and polarity changes appear to take place in the RPE of *p27^{Kip1}*-null animals. Whether these changes are intrinsic to the epithelium or arise as a result of modifications secondary to those occurring within the retina is not clear. In any event, a better understanding of these issues may shed light on the processes contributing to retinal detachment.

Recently, it has been shown that, in addition to its well-established role as an inhibitor of nuclear cyclin-Cdk complexes, p27^{Kip1} performs an important cytosolic function as a regulator of actin dynamics and cell migration [35,36]. Interestingly, *p27^{Kip1}*-deficient fibroblasts have decreased motility and display increased numbers of stress fibers and focal adhesions, compared to wild-type cells [36,37]. Reintroduction into *p27^{Kip1}*-deficient cells of either a wild-type *p27^{Kip1}* gene, or a gene encoding a *p27^{Kip1}* mutant with impaired binding to cyclin-Cdks, significantly decreased the number of stress fibers and focal adhesions. Furthermore, it has been shown by Besson et al. [37] that the C-terminal domain of the protein is able to bind to, and inhibit activation of, the small GTP-ase RhoA in vitro. Thus, the accumulated evidence indicates that p27^{Kip1} acts as a negative regulator of the RhoA pathway through a portion of the protein distinct from its cyclin-Cdk binding domain. While the RPE is not normally migratory, loss of p27^{Kip1} could nevertheless have an effect on the arrangement or contractility of the epithelial actin cytoskeleton that might influence its interaction with the neural retina. These issues need to be examined directly in future studies.

ACKNOWLEDGEMENTS

Supported by Grants EY14559 (DMD) and EY13760 (EML) from NIH, and by a Career Development Grant from Research to Prevent Blindness and a grant from The Foundation Fighting Blindness (to EML). We also wish to thank Ms. Judy Whittimore for help with electron microscopy. The authors have no financial interest in this project. This research was presented in part on May 2, 2005 at the annual meeting of the Association for Research in Vision and Ophthalmology (ARVO), Fort Lauderdale, FL (abstract E-1635).

REFERENCES

1. Bok D. The retinal pigment epithelium: a versatile partner in vision. J Cell Sci Suppl 1993; 17:189-95.
2. Boulton M, Dayhaw-Barker P. The role of the retinal pigment epithelium: topographical variation and ageing changes. Eye 2001; 15:384-9.
3. Morris DA, Henkind P. Pathological responses of the human retinal pigment epithelium. In: Zinn KM, Marmor MF, editors. The Retinal pigment epithelium. Cambridge (MA): Harvard University Press; 1979. p. 247-66.
4. Sarks SH, Sarks JP. Age-related macular degeneration: atrophic form. In: Ryan SJ, editor. Retina. 2nd ed. Vol II. St. Louis: Mosby; 1994. p. 1071-102.
5. Morgan DO. Cyclin-dependent kinases: engines, clocks, and microprocessors. Annu Rev Cell Dev Biol 1997; 13:261-91.
6. Sherr CJ, Roberts JM. Living with or without cyclins and cyclin-dependent kinases. Genes Dev 2004; 18:2699-711.
7. Sherr CJ. The Pezcoller lecture: cancer cell cycles revisited. Cancer Res 2000; 60:3689-95.
8. Sherr CJ, Roberts JM. CDK inhibitors: positive and negative regulators of G_1-phase progression. Genes Dev 1999; 13:1501-12.
9. Sherr CJ, Roberts JM. Inhibitors of mammalian G_1 cyclin-dependent kinases. Genes Dev 1995; 9:1149-63.
10. Nakayama K, Nakayama K. Cip/Kip cyclin-dependent kinase inhibitors: brakes of the cell cycle engine during development. Bioessays 1998; 20:1020-9.
11. Conlon I, Raff M. Size control in animal development. Cell 1999; 96:235-44.
12. Durand B, Fero ML, Roberts JM, Raff MC. p27^{Kip1} alters the response of cells to mitogen and is part of a cell-intrinsic timer that arrests the cell cycle and initiates differentiation. Curr Biol 1998; 8:431-40.
13. Durand B, Raff M. A cell-intrinsic timer that operates during oligodendrocyte development. Bioessays 2000; 22:64-71.
14. Fero ML, Rivkin M, Tasch M, Porter P, Carow CE, Firpo E, Polyak K, Tsai LH, Broudy V, Perlmutter RM, Kaushansky K, Roberts JM. A syndrome of multiorgan hyperplasia with features of gigantism, tumorigenesis, and female sterility in p27^{Kip1}-deficient mice. Cell 1996; 85:733-44.
15. Kiyokawa H, Kineman RD, Manova-Todorova KO, Soares VC, Hoffman ES, Ono M, Khanam D, Hayday AC, Frohman LA, Koff A. Enhanced growth of mice lacking the cyclin-dependent kinase inhibitor function of p27^{Kip1}. Cell 1996; 85:721-32.
16. Nakayama K, Ishida N, Shirane M, Inomata A, Inoue T, Shishido N, Horii I, Loh DY, Nakayama K. Mice lacking p27^{Kip1} display increased body size, multiple organ hyperplasia, retinal dyspla-

sia, and pituitary tumors. Cell 1996; 85:707-20.
17. Levine EM, Close J, Fero M, Ostrovsky A, Reh TA. p27Kip1 regulates cell cycle withdrawal of late multipotent progenitor cells in the mammalian retina. Dev Biol 2000; 219:299-314.
18. Dyer MA, Cepko CL. Control of Muller glial cell proliferation and activation following retinal injury. Nat Neurosci 2000; 3:873-80.
19. Kogan SC, Doherty M, Gitschier J. An improved method for prenatal diagnosis of genetic diseases by analysis of amplified DNA sequences. Application to hemophilia A. N Engl J Med 1987; 317:985-90.
20. Chen W, Joos TO, Defoe DM. Evidence for β1-integrins on both apical and basal surfaces of Xenopus retinal pigment epithelium. Exp Eye Res 1997; 64:73-84.
21. Gavrieli Y, Sherman Y, Ben-Sasson SA. Identification of programmed cell death in situ via specific labeling of nuclear DNA fragmentation. J Cell Biol 1992; 119:493-501.
22. Defoe DM, Easterling KC. Reattachment of retinas to cultured pigment epithelial monolayers from Xenopus laevis. Invest Ophthalmol Vis Sci 1994; 35:2466-76.
23. Bodenstein L, Sidman RL. Growth and development of the mouse retinal pigment epithelium. I. Cell and tissue morphometrics and topography of mitotic activity. Dev Biol 1987; 121:192-204.
24. Yoshida K, Kase S, Nakayama K, Nagahama H, Harada T, Ikeda H, Harada C, Imaki J, Ohgami K, Shiratori K, Ilieva IB, Ohno S, Nishi S, Nakayama KI. Involvement of $p27^{KIP1}$ in the proliferation of the developing corneal endothelium. Invest Ophthalmol Vis Sci 2004; 45:2163-7.
25. Bora N, Defoe D, Smith SB. Evidence of decreased adhesion between the neural retina and retinal pigmented epithelium of the *Mitf*^{vit} (*vitiligo*) mutant mouse. Cell Tissue Res 1999; 295:65-75.
26. Nandrot EF, Anand M, Sircar M, Finnemann SC. Novel role for αvβ5-integrin in retinal adhesion and its diurnal peak. Am J Physiol Cell Physiol 2006; 290:C1256-62.
27. Defoe DM, Levine EM. Expression of the cyclin-dependent kinase inhibitor p27Kip1 by developing retinal pigment epithelium. Gene Expr Patterns 2003; 3:615-9.
28. Caviness VS Jr, Goto T, Tarui T, Takahashi T, Bhide PG, Nowakowski RS. Cell output, cell cycle duration and neuronal specification: a model of integrated mechanisms of the neocortical proliferative process. Cereb Cortex 2003; 13:592-8.
29. Yoshida K, Nakayama K, Kase S, Nagahama H, Harada T, Ikeda H, Harada C, Imaki J, Ohgami K, Shiratori K, Ohno S, Nishi S, Nakayama KI. Involvement of p27(KIP1) in proliferation of the retinal pigment epithelium and ciliary body. Anat Embryol (Berl) 2004; 208:145-50.
30. Stroeva OG, Mitashov VI. Retinal pigment epithelium: proliferation and differentiation during development and regeneration. Int Rev Cytol 1983; 83:221-93.
31. Yoshida K, Kase S, Nakayama K, Nagahama H, Harada T, Ikeda H, Harada C, Imaki J, Ohgami K, Shiratori K, Ohno S, Nakayama KI. Distribution of p27(KIP1), cyclin D1, and proliferating cell nuclear antigen after retinal detachment. Graefes Arch Clin Exp Ophthalmol 2004; 242:437-41.
32. Ameen NA, Salas PJ. Microvillus inclusion disease: a genetic defect affecting apical membrane protein traffic in intestinal epithelium. Traffic 2000; 1:76-83.
33. Vega-Salas DE, Salas PJ, Rodriguez-Boulan E. Exocytosis of vacuolar apical compartment (VAC): a cell-cell contact controlled mechanism for the establishment of the apical plasma membrane domain in epithelial cells. J Cell Biol 1988; 107:1717-28.
34. Bonilha VL, Rayborn ME, Saotome I, McClatchey AI, Hollyfield JG. Microvilli defects in retinas of ezrin knockout mice. Exp Eye Res 2006; 82:720-9.
35. Nagahara H, Vocero-Akbani AM, Snyder EL, Ho A, Latham DG, Lissy NA, Becker-Hapak M, Ezhevsky SA, Dowdy SF. Transduction of full-length TAT fusion proteins into mammalian cells: TAT-$p27^{Kip1}$ induces cell migration. Nat Med 1998; 4:1449-52.
36. McAllister SS, Becker-Hapak M, Pintucci G, Pagano M, Dowdy SF. Novel $p27^{kip1}$ C-terminal scatter domain mediates Rac-dependent cell migration independent of cell cycle arrest functions. Mol Cell Biol 2003; 23:216-28.
37. Besson A, Gurian-West M, Schmidt A, Hall A, Roberts JM. $p27^{kip1}$ modulates cell migration through the regulation of RhoA activation. Genes Dev 2004; 18:862-76.

The print version of this article was created on 27 Feb 2007. This reflects all typographical corrections and errata to the article through that date. Details of any changes may be found in the online version of the article.